Ding *et al.*
Protection and Control of Modern Power Systems (2022) 7:49
https://doi.org/10.1186/s41601-022-00270-x

Protection and Control of Modern Power Systems

ORIGINAL RESEARCH

Open Access

A demand side controller of electrolytic aluminum industrial microgrids considering wind power fluctuations

Xin Ding[1,2], Jian Xu[1*], Yuanzhang Sun[1], Siyang Liao[1] and Jingwen Zheng[3]

Abstract

Direct wind power purchase for large industrial users is a meaningful way to improve wind power consumption and decrease industrial production costs. Short-term wind power fluctuations may lead to large-scale wind power curtailment problems. To promote use of wind energy, a demand side control method is proposed based on output regulator theory for a grid-connected industrial microgrid with electrolytic aluminum loads to continuously track and respond to wind power fluctuations. The control model of the EALs and the dominant frequencies of the wind power fluctuation signals are analyzed and incorporated into the demand side control plant. The feedback control signals with active power deviations on the tie-line are used to design the demand side controller. Simulations are conducted for an actual industrial microgrid to validate the feasibility and effectiveness of the proposed method. The results demonstrate that the proposed controller based on output regulator theory is able to effectively track wind power fluctuations.

Keywords: Wind power fluctuations, Electrolytic aluminum load, Demand side control, Output regulator theory, Industrial microgrid

1 Introduction

To deal with energy shortage and environmental pollution, the government of China is actively promoting the construction of a low-carbon energy system. With the growing demand for energy saving and emission reduction, wind power is playing an increasingly important role in modern power systems. As a result, installed capacity of wind power has increased rapidly in China. According to the National Energy Administration, by the end of 2021, the installed wind power capacity in China has reached 328.48 GW, representing a 16.6% increase on 2020 [1]. In China, wind power resources are mainly concentrated in the northeastern, northern and northwestern regions with 61.9% of the total installed wind power capacity. However, wind power utilization is a serious issue [2]. In 2021, the lost electricity caused by wind power curtailment in northern and northwestern regions accounted for 13.0% and 26.6%, respectively, which was huge waste of investment and resource.

The reasons for large-scale wind power curtailment can be summarized as: (1) The locations of wind resources (most in northern and western regions) and load centers (most in eastern and southeastern regions) in China are distributed inversely, while lacking reserve capacity results in restriction on long-distance cross-regional wind power transmission [3]; (2) The imbalance between power supply and demand in local regions leads to wind power redundancy [4].

To alleviate the problems of local wind power consumption, the Chinese government has started to implement policies, such as lower electricity price, to encourage energy-intensive industrial production in those areas with abundant wind energy resources [5],

*Correspondence: xujian@whu.edu.cn

[1] School of Electrical Engineering and Automation, Wuhan University, Wuhan 430072, China
Full list of author information is available at the end of the article

Springer Open

© The Author(s) 2022. **Open Access** This article is licensed under a Creative Commons Attribution 4.0 International License, which permits use, sharing, adaptation, distribution and reproduction in any medium or format, as long as you give appropriate credit to the original author(s) and the source, provide a link to the Creative Commons licence, and indicate if changes were made. The images or other third party material in this article are included in the article's Creative Commons licence, unless indicated otherwise in a credit line to the material. If material is not included in the article's Creative Commons licence and your intended use is not permitted by statutory regulation or exceeds the permitted use, you will need to obtain permission directly from the copyright holder. To view a copy of this licence, visit http://creativecommons.org/licenses/by/4.0/.

e.g., the "Direct power purchase for large industrial users" policy since 2002 [6]. In the meantime, industrial enterprises are happy to look for ways of saving cost and promoting economic benefits. Thus, large industrial users have agreed to purchase electricity directly from an energy generator by signing long-term "power purchase agreement" contracts. This is different from the traditional way of buying electricity from a utility power grid [7]. Such policies are carried out by direct negotiation between generation and large users. These have made some progress in promoting power market reform in China. Over the last decade, the fast developing renewable energy generation and coordination with thermal power generation have been considered for the establishment of the electricity market [8, 9].

However, large-scale wind power fluctuations may bring negative effects on carrying out "direct wind power purchase (DWPP)" policies. Normally, energy storage systems (ESS) are applied to smooth wind power fluctuations [10], although the construction of large-scale ESS will increase investment cost for the power grid. In addition, industrial users may purchase extra reserve power instead of fluctuating wind power, and this is against the intention of DWPP to save production costs.

Some energy-intensive industrial loads with heat storage characteristics, such as electrolytic aluminum loads (EALs), have hundreds of megawatt power capacity. The demand side control methods and auxiliary service of EALs have been much studied. The analytical studies suggest that the EALs can help smooth the wind fluctuation in those grid-connected industrial microgrid (IMG) that have high penetration of wind power by using the tie-line active power deviation as the feedback signal [11, 12]. In an actual isolated industrial power system in China, the EALs are regulated to maintain frequency stability via controlling the generator excitation voltage or the saturable reactors of the EALs [13, 14]. With these control methods, the experimental verification of EALs in an actual IMG for primary frequency control is analyzed and discussed [15]. A hierarchical framework is proposed to coordinate the EALs and thermal power plants in an industrial park for secondary frequency regulation [16]. The results show that EALs offer huge regulating potential to respond to wind power fluctuations in the context of DWPP for large industrial users.

Remote wind power fluctuations tracking problems for large industrial users are significant and need to be explored. EALs are normally placed in a microgrid with a mature communication system. This serves as a foundation for demand side control. In addition, EALs are able to carry out continuous active power modulation with large regulation capacity for direct load control. The industrial microgrid is connected with the utility power grid (UPG) via the tie-line, developing the regulating potentials of EALs to track that the short-term wind power fluctuations are meaningful for carrying out the DPPU policies. Thus, wind power tracking can be discussed as power management problems on the tie-line and demand side.

The existing literature on power flow control of tie-line mainly focuses on long-term time-scales. An optimized fuzzy logic controller is proposed in [17] to minimize the daily tie-line power flow in a grid-connected microgrid with PV and ESS. In [18], an adaptive robust tie-line scheduling system considering wind power uncertainty is presented to optimize tie-line power flows every 15 min while a coordination control algorithm is developed to smooth tie-line power with a time interval of 10 min [19]. However, the previously mentioned studies do not cover the detailed dynamic model of the demand side. Thus, the strategies in [17–19] may be difficult to apply for dealing with short-term tie-line power fluctuations (5 min or less). In addition, wind power fluctuations appear as time-varying disturbance signals. Consequently, the traditional PI or PID controllers in [20, 21] are incapable of achieving zero steady-state error control effectively in terms of tracking wind power fluctuations on the demand side.

This paper aims to develop a theoretically sound and practically feasible demand side controller for EALs, one which guarantees wind power tracking for an electrolytic aluminum IMG. Using the theoretical development in [22, 23], output regulator theory is applied to design the feedback controller to solve the tracking or rejecting issues for the output in a control system. This has been verified to give satisfactory performance for demand side control in [12, 13].

The main contributions of the paper are:

1. A wide area closed-loop demand side control architecture is proposed to dynamically modulate the power consumption of EALs in an IMG. The advantages of regulating EALs are also illustrated. A direct wind power purchasing structure for an electrolytic aluminum IMG is discussed in detail to encourage wind power plants and industrial users to participate in DWPP policies.
2. A demand side controller based on output regulator theory is developed to achieve zero steady-state error in tracking short-term wind power fluctuations and satisfactory dynamic performance of the controlled EALs. The proposed controller only needs local state variables and a remote disturbance signal, instead of the network configuration of the UPG.

The rest of the paper is organized as follows. Section 2 describes the research background of an actual IMG and the direct wind power purchasing structure. The demand side control method of aluminum loads is presented in Sect. 3 while Sect. 4 introduces a demand side controller based on regulator theory and its design procedure. The simulation results conducted on the actual industrial microgrid are presented in Sect. 5, and conclusions are given in Sect. 6.

2 Direct wind power purchasing structure of an actual grid-connected IMG

2.1 Background of the electrolytic aluminum IMG

Normally, high energy consumption industrial loads, such as electrolytic aluminum productions, are placed in an industrial park, whose typical structure is shown in Fig. 1. As shown, the IMG is connected with the UPG via a tie-line.

Because of high energy consumption, the electricity cost for electrolytic aluminum enterprises may account for 30% to 40% of the total production cost [24]. Therefore, seeking generation sources with lower electricity fees brings economic significance to large industrial consumers. As shown in Fig. 1, the local thermal plants supply power directly to the aluminum loads instead of transmitting to the UPG, while the UPG covers the power imbalance between the local thermal plants and the large industrial consumers. The UPG also supplies reserve power when short circuit faults occur in the IMG. In summary, the electrical energy that the EALs need is from two sources: the local thermal plants and the UPG.

In the context of DWPP, industrial users are able to sign the power purchase contract with the wind power plants and power grid, while the direct purchase price is set lower than the grid sale price. Thus, for the electrolytic aluminum enterprises, directly purchasing wind power can decrease the production cost. Additionally, such a trading mechanism is profitable and improves the economic benefits of wind power retailers and promotes renewable energy consumption.

To promote renewable energy use, wind power is transmitted to the power grid in combination with thermal power. The active power on the tie-line P_{tie} is the purchasing power between the IMG and UPG. Normally, the IMG makes contracts with wind power plants and the UPG based on the negotiated trading electricity and transmission fee, while the randomness and volatility of the wind power (especially in extreme scenarios) are dismissed. Since EALs are able to regulate their power consumption, it is meaningful for the demand side to respond to the wind power fluctuations, and this can be presented as obvious performance for DWPP. Therefore, it is vital to develop a practical control method for electrolytic aluminum enterprises to realize wind power tracking.

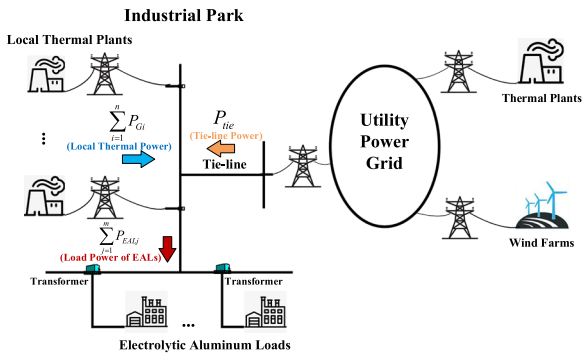

Fig. 1 The structure of an industrial park with EALs

2.2 Wide area closed-loop demand side control

Assuming that an IMG contains n local generators and m EALs, the active power relation between generation and demand sides in an IMG is expressed as

$$\sum_{i=1}^{n} P_{Gi} + P_{tie} = \sum_{j=1}^{m} P_{EALj} + P_{hot} + P_{loss} \tag{1}$$

where P_{Gi} is the output power of the ith generator. P_{EALj} and P_{hot} are the active power consumption of the jth EAL and heating loads, respectively. P_{loss} is the active power loss of the IMG, while P_{tie} is the transmission power on the tie-line, which is connected to the IMG and UPG.

The heating loads P_{hot} and the active power loss P_{loss} are considered as constant loads. Theoretically, the power change of the EALs leads to the change of P_{tie} and P_{Gi}, which can be described as:

$$\sum_{i=1}^{n} \Delta P_{Gi} + \Delta P_{tie} = \sum_{j=1}^{m} \Delta P_{EALj} \tag{2}$$

By using spectrum analysis, the remote wind power fluctuation ΔP_w can be classified into low and high-frequency types. These characterize slow and violent fluctuations, respectively. The active power of the EALs can be regulated at the milliseconds level, which is much faster than the regulation of local thermal generators, while for slow wind fluctuations, the thermal generators are able to respond. In this paper, extreme wind power fluctuation scenarios are considered, and at the seconds level, the active power of thermal generators is considered to be constant. Thus, in practice, (2) can be simplified to:

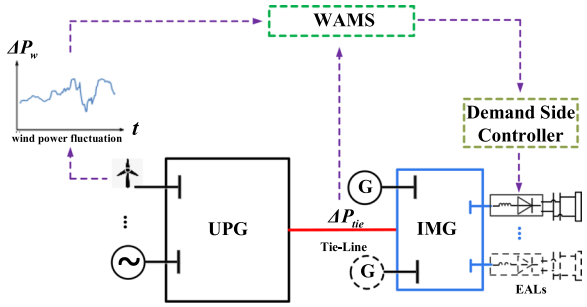

Fig. 2 The wide area closed-loop demand side control architecture with the application of WAMS

$$\Delta P_{tie} \approx \sum_{j=1}^{m} \Delta P_{EALj} \tag{3}$$

Based on (3), ΔP_{tie} changes correspondingly when the EALs are regulated to respond to wind power fluctuations. This could be presented as the case that electrolytic aluminum enterprises directly purchase wind power.

Figure 2 presents a wide area closed-loop demand side control architecture. With the help of a wide area measurement system (WAMS) [24], the wide area demand side control is able to be carried out in extreme wind power fluctuating scenarios (at the seconds level). The remote wind power fluctuation signal ΔP_w can be measured in real-time by PMUs and delivered to the demand side controller via fast communication channels. The output signals of the demand side controller can activate to regulate the power consumption of the EALs ΔP_{EALj}.

In practical application, the WAMS control station, downlink channel and the network control units (NCU) are necessary for the wide area closed-loop demand side control system [25]. The WAMS control station communicates with the PMUs via the transmission control protocol/Internet Protocol (TCP/IP) to monitor the status of the power system. The WAMS control station also calculates the demand side controllers based on the system status sent by the PMUs and sends the control parameters to the NCUs, while the NCUs issue the control commands to regulate the active power consumptions of the EALs, ΔP_{EALj}.

As a result, the active power fluctuation on the tie-line, ΔP_{tie}, can be controlled to correspond with ΔP_w according to (1)–(3). Consequently, the active power deviation signal ΔP_{tie} can be monitored to compare with ΔP_w. This means that the electrolytic aluminum consumers purchase the electricity from the wind power generation enterprises.

The basic principle of the proposed control method can be summarized as: the power deviation signal ΔP_{tie} is regulated to track the reference signal ΔP_w by controlling the power consumption P_{EAL}. The proposed demand side control is considered as a wide-area control scheme since the remote information is used as the feedback signal. In addition, the demand control architecture is formulated as a closed-loop control system. This will be discussed in detail in Sect. 4.1.

From the above analysis, the key issue is how to control the EALs. To implement the demand side control scheme, the characteristics of the EALs are analyzed in detail in the next section.

3 Control method of EALs

3.1 Equivalent model of EALs

The configuration and operational characteristics of the EALs have been discussed in detail in [14]. Figure 3 depicts the electrical diagram and its equivalent circuit of an EAL. The electrolyzing production is driven by the DC voltage U_{DC}, generated by twelve full-bridge rectifiers with saturable reactors. All the electrolytic cells are in series and can be represented by a back electromotive force (emf) E and a resistance R. From the experimental results, the equivalent back emf E is 354.6 V and the resistance R is 2.016 mΩ [14]. In Fig. 3, U_{AC} and k are the load bus voltage and the transformer ratio, respectively. U_{SR} is the voltage drop on the saturable reactor, with the nominal value of 20–40 V (maximum value allowed 60–70 V).

The active power consumption of the EAL P_{EAL} is deduced in [14, 15], as:

$$P_{EAL} = U_{DC} I_{DC} = (I_{DC} R + E) I_{DC} \tag{4}$$

where I_{DC} is the direct current which can be expressed by:

$$I_{DC} = \frac{U_{DC} - E}{R} = \frac{1.35\left(U_{AC}/k - U_{SR}\right) - E}{R} \tag{5}$$

Equation (4) indicates that the active power of the aluminum load P_{EAL} is related to the direct current I_{DC}. Based on (5), there are two methods for regulating P_{EAL}

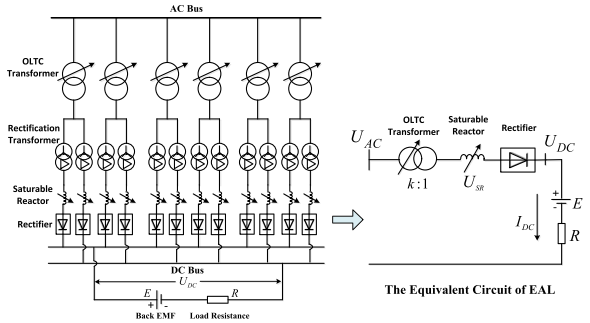

Fig. 3 The electrical diagram and the equivalent circuit of the EAL

in actual production, i.e., regulating the tap changer of the OLTC (i.e., the value of k) or adjusting the voltage drop U_{SR} on the saturable reactor by controlling the inductance value L_{SR} [14]. Because of the advantages of fast response (milliseconds) and continuous regulation, controlling U_{SR} is better for responding to wind power fluctuation.

3.2 Control method of EAL

Based on (4) and (5), P_{EAL} is relevant to I_{DC} which is controlled by regulating the value of U_{SR}. Figure 4 depicts a DC side current control model in actual production.

In Fig. 4, I_{DC0} and I_{DCref} are the initial value and reference of the DC side current, respectively. ΔI_{DC}, as the control input of the model, is the DC side current deviation. T_{DC} and T_{SR} are the time constants of the control model, while K_P, K_I and K_{SR} are the gain coefficients. ΔU_{SR} is the voltage deviation on the saturable reactor, with the maximal and minimal values expressed as ΔU_{SRmax} and ΔU_{SRmin}.

According to Fig. 4, for the jth EAL, the dynamic equations are given by:

$$\begin{cases} T_{DCj}\Delta\dot{I}_{DCaj} = -\Delta I_{DCaj} + \Delta I_{DCrefj} \\ \Delta\dot{I}_{DCbj} = \left(-K_{pj}/T_{DCj} + K_{Ij}\right)\Delta I_{DCaj} + \left(K_{pj}/T_{DCj}\right)\Delta I_{DCrefj} \\ T_{SRj}\Delta\dot{U}_{SRj} = K_{SRj}\Delta I_{DCbj} - \Delta U_{SRj} \end{cases} \tag{6}$$

Combining (4)–(5), the active power deviation of the EAL ΔP_{EALj} can be calculated by:

$$\Delta P_{EALj} = \left[1.35\Delta U_{SRj}\left(1.35\Delta U_{SRj} - 2U_{DC0j} + E_j\right)\right]/R_j \tag{7}$$

where U_{DC0j} is the initial value of the DC side voltage.

Based on (3) and (7), ΔP_{tie} can be determined by:

$$\Delta P_{tie} = \sum_{j=1}^{m} \Delta P_{EALj} = \sum_{j=1}^{m} \left(a_j \Delta U_{SRj}^2 + b_j \Delta U_{SRj}\right) \tag{8}$$

where a_j and b_j are the coefficients of the quadratic terms and linear terms, respectively.

Based on the discussion above, the aluminum load control possesses the following advantages in responding to wind power fluctuation:

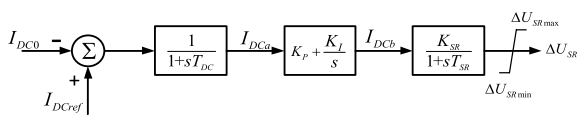

Fig.4 A direct side current control model of EAL

1. *Fast Response.* The power consumption of the EALs can be regulated continuously by adjusting the saturable reactors within tens of milliseconds. Thus, the demand side can be controlled at the seconds level, which is sufficient for extreme wind power fluctuation scenarios.
2. *Considerable Regulating Capacity.* The EALs' active power consumption can be modulated over the range of − 10% to + 5% by regulating ΔU_{SR} within its operating limits (20–70 V). This is considerable potential regulating capacity due to their large power consumption. The regulation shows no obvious negative effect on the aluminum production if the temperature of electrolytic cells can be kept within the acceptable range [14].

As this paper concentrates on the demand side control in an IMG to track wind fluctuation in a remote area, the remainder of the paper will focus on the issue of how to develop a theoretically sound and practically feasible demand side controller using remote information.

4 Demand side control based on output regulator theory

The aim of the demand side control scheme is to regulate the active power on the tie-line to track wind power fluctuations by controlling the voltage drop on the saturable reactors. The proposed control strategy indicates that ΔP_w exists as a time-varying disturbance signal from the exogenous system and ΔP_{tie} represents the output signal of the control system. Traditional control methods such as PI and PID controllers are incapable of realizing tracking wind power fluctuation effectively. It is worth noting that such a demand side control problem can be reformulated as an output regulation problem. Consequently, the active power regulation problem of EALs can be solved using output regulator theory [22, 23].

4.1 Demand side control model

The demand side controller for the EALs [seen as (3), (6), (7) and (8)] can be described in a linearization form:

$$\begin{cases} \dot{\boldsymbol{x}} = \boldsymbol{A}\boldsymbol{x} + \boldsymbol{B}\boldsymbol{u} + \boldsymbol{P}\boldsymbol{d} \\ \dot{\boldsymbol{d}} = \boldsymbol{S}\boldsymbol{d} \\ \boldsymbol{e} = \boldsymbol{y} - \boldsymbol{y}_r = \boldsymbol{C}\boldsymbol{x} + \boldsymbol{Q}\boldsymbol{d} \end{cases} \tag{9}$$

In (9), the first equation describes a controlled plant with the system state $\boldsymbol{x} \in \boldsymbol{R}^r$, control input $\boldsymbol{u} \in \boldsymbol{R}^p$ and external signal $\boldsymbol{d} \in \boldsymbol{R}^s$. The second equation represents an exosystem with disturbances (to be rejected) or references (to be tracked), while the third equation defines an error variable $\boldsymbol{e} \in \boldsymbol{R}^q$ between the output $\boldsymbol{y} = \boldsymbol{C}\boldsymbol{x}$ and the reference $\boldsymbol{y}_r = -\boldsymbol{Q}\boldsymbol{d}$. The detailed diagram of the closed-loop control system is presented in Fig. 5.

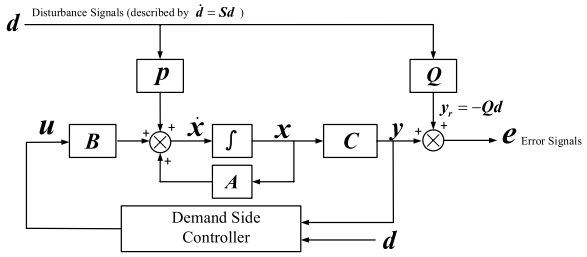

Fig.5 Block diagram of the demand side control plant

Assuming an IMG with m EALs, the control system (6) is of the form (9), where the state $\boldsymbol{x} = [\Delta \boldsymbol{I}_{\boldsymbol{DCaj}}, \Delta \boldsymbol{I}_{\boldsymbol{DCbj}}, \Delta \boldsymbol{U}_{\boldsymbol{SRj}}] \in \boldsymbol{R}^{3m}$, control input $\boldsymbol{u} = \Delta \boldsymbol{I}_{\boldsymbol{DCrefj}} \in \boldsymbol{R}^{m}$, external disturbance signal $\boldsymbol{d} = \Delta \boldsymbol{P}_{\boldsymbol{w}} \in \boldsymbol{R}$. The aim of the demand side control scheme is to regulate the power deviation on the tie-line ΔP_{tie} to respond to the wind power fluctuation ΔP_w by controlling the power consumption of the EALs. The output $\boldsymbol{y}$ and the reference signal $-\boldsymbol{y}_{\boldsymbol{r}}$ in the proposed control strategy are ΔP_{tie} and ΔP_w, respectively.

From (8), ΔP_{tie} is presented as a nonlinear expression with ΔU_{SRj} in the form $\boldsymbol{y} = \boldsymbol{h}(\boldsymbol{x})$. Note that the quadratic terms have a very low impact on the value of ΔP_{tie} (lower than the 3% of total ΔP_{EALj} while the saturable reactors are regulated to their limits), for the convenience of designing the feedback controller, (8) is linearized into $\boldsymbol{y} = \boldsymbol{Cx}$ with $\boldsymbol{C} = [\partial \boldsymbol{h}/\partial \boldsymbol{x}]_{x=0}$. Hence, the matrices $(\boldsymbol{A}, \boldsymbol{B}, \boldsymbol{C})$ are given as follows:

$$\boldsymbol{A} = \begin{bmatrix} -\frac{\mathbf{1}}{\boldsymbol{T_{DCj}}} & \mathbf{0} & \mathbf{0} \\ -\frac{\boldsymbol{K_{Pj}}}{\boldsymbol{T_{DCj}}} + \boldsymbol{K_{Ij}} & \mathbf{0} & \mathbf{0} \\ \mathbf{0} & \frac{\boldsymbol{K_{SRj}}}{\boldsymbol{T_{SRj}}} & -\frac{\mathbf{1}}{\boldsymbol{T_{SRj}}} \end{bmatrix} \in \boldsymbol{R}^{3m\times 3m},$$

$$\boldsymbol{B} = \begin{bmatrix} 1/\boldsymbol{T_{DCj}} \\ \boldsymbol{K_{Pj}}/\boldsymbol{T_{DCj}} \\ \mathbf{0} \end{bmatrix} \in \boldsymbol{R}^{3m\times m}$$

$$\boldsymbol{C} = \begin{bmatrix} \mathbf{0} & \mathbf{0} & \boldsymbol{b_j} \end{bmatrix} \in \boldsymbol{R}^{1\times 3m},\ b_j = \frac{1.35\left(-2U_{DC0j} + E_j\right)}{R_j}$$

The exosystem matrix $\boldsymbol{S}$ is formulated to describe the dynamic characteristic of the external signal. Here, the wind power fluctuation ΔP_w is considered as a time-varying function, which can be described by the sinusoidal time varying signals, as [26]:

$$\Delta P_w(t) = A_0 + \sum_{n=1}^{\infty} B_n \sin\left(\omega_n t + \varphi_n\right) \tag{10}$$

Neglecting the high order terms, ΔP_w can be approximated by:

$$\Delta P_w(t) \approx A_0 + \sum_{n=1}^{N} B_n \sin\left(\omega_n t + \varphi_n\right) \tag{11}$$

We use $(\boldsymbol{d_{n1}}, \boldsymbol{d_{n2}}, \boldsymbol{d_0})$ to represent each component in (11), expressed as:

$$\begin{aligned} \boldsymbol{d_{n1}} &= B_n \sin\left(\omega_n t + \varphi_n\right) \\ \boldsymbol{d_{n2}} &= B_n \cos\left(\omega_n t + \varphi_n\right) \\ \boldsymbol{d_0} &= A_0 \end{aligned} \tag{12}$$

The first-order derivatives of $\boldsymbol{d_{n1}}$ and $\boldsymbol{d_{n2}}$ are:

$$\begin{bmatrix} \dot{\boldsymbol{d}}_{\boldsymbol{n1}} \\ \dot{\boldsymbol{d}}_{\boldsymbol{n2}} \end{bmatrix} = \begin{bmatrix} 0 & \omega_n \\ -\omega_n & 0 \end{bmatrix} \begin{bmatrix} \boldsymbol{d_{n1}} \\ \boldsymbol{d_{n2}} \end{bmatrix} \tag{13}$$

We denote that $\boldsymbol{d} = (\boldsymbol{d}_{11}, \boldsymbol{d}_{12}, \ldots, \boldsymbol{d_{N1}}, \boldsymbol{d_{N2}}, \boldsymbol{d_0})^{\mathrm{T}}$ so that the exosystem model can be expressed by:

$$\dot{\boldsymbol{d}} = \boldsymbol{Sd} = \begin{bmatrix} \omega_1 \boldsymbol{S}_0 & \cdots & \mathbf{0} & \mathbf{0} \\ \vdots & \ddots & \vdots & \vdots \\ \mathbf{0} & \cdots & \omega_n \boldsymbol{S}_0 & \mathbf{0} \\ \mathbf{0} & \cdots & \mathbf{0} & \mathbf{0} \end{bmatrix},\ \boldsymbol{dS}_0 = \begin{bmatrix} 0 & 1 \\ -1 & 0 \end{bmatrix} \tag{14}$$

It is worth noting that the exosystem matrix $\boldsymbol{S}$ is formulated by only the angular frequency ω_n and not with the magnitude A_0, B_n and the phase φ_n. Therefore, the dynamic equation of the disturbance characteristic can be given by (14) once the dominant frequencies of the disturbance signal ΔP_w are obtained by applying a Fourier transform.

For the error equation in (9), the deviation between ΔP_{tie} and ΔP_w is selected as the error signal $\boldsymbol{e}$ (i.e., $\boldsymbol{e} = \Delta P_{tie} - \Delta P_w$), in the form of $\boldsymbol{e} = \boldsymbol{Cx} + \boldsymbol{Qd}$. Consequently, the pair $(\boldsymbol{P}, \boldsymbol{Q})$ can be deduced as:

$$\boldsymbol{P} = \mathbf{0}\boldsymbol{Q} = \begin{bmatrix} -1 & 0 & \cdots & -1 & 0 & -1 \end{bmatrix} \in \boldsymbol{R}^{1\times(2N+1)}$$

The purpose of the demand side control scheme is to realize zero error by regulating the power consumption of the EALs in the IMG. This can be naturally formulated as an output regulation problem. In the next subsection, output regulator theory is introduced to design the feedback controller.

4.2 Output regulator theory

The control objective of the demand side control scheme is to achieve error regulation and maintain the internal stability of the system. For the control system in (9), it finds, if possible, the gain matrices $\boldsymbol{K} \in \boldsymbol{R}^{p\times r}$ and $\boldsymbol{L} \in \boldsymbol{R}^{p\times s}$ to design the full-information feedback controller of the form

$$\boldsymbol{u} = \boldsymbol{Kx} + \boldsymbol{Ld} \tag{15}$$

such that the following two requirements are satisfied:

R1) Internal stability. When $\boldsymbol{d} = \boldsymbol{0}$, the closed-loop system $\dot{\boldsymbol{x}} = (\boldsymbol{A} + \boldsymbol{BK})\boldsymbol{x}$ is asymptotically stable, i.e., find the gain matrix $\boldsymbol{K}$ such that $\sigma(\boldsymbol{A} + \boldsymbol{BK}) \subseteq \mathbb{C}^-$;
R2) Error regulation. When $\boldsymbol{d} \neq \boldsymbol{0}$, for every initial condition $(\boldsymbol{x_0}, \boldsymbol{d_0})$, the closed-loop system (8)–(9) satisfies $\lim_{t\to\infty} \boldsymbol{e}(t) = 0$.

In order to maintain I_{DCrefj} of the EALs in the permitted range, the constraints of the EALs have to be considered. Thus,
$\lim_{t\to\infty} e(t) = 0$ subjecting to (9) and $|u_j| \le u_{max}$, $j = 1, 2, \ldots, m$.
where u_j is the jth element of $\boldsymbol{u}$ and u_{max} is the bound of $|u_j|$.

To solve the output regulator problem, the following assumptions are required:

A1) all the eigenvalues of the matrix $\boldsymbol{S} \in \boldsymbol{R}^{s\times s}$ are located on the closed right-half plane.
A2) the pair $(\boldsymbol{A}, \boldsymbol{B})$ is stabilizable.
A3) the pair $\left(\begin{bmatrix} \boldsymbol{A} & \boldsymbol{P} \\ \boldsymbol{0} & \boldsymbol{S} \end{bmatrix}, \begin{bmatrix} \boldsymbol{C} & \boldsymbol{Q} \end{bmatrix}\right)$ is detectable.

Reference [24] proves a necessary and sufficient condition for the solvability of the output regulator problem. Supposing *A1)* and *A2)* hold, the output regulation problem is solvable by full-information feedback if and only if there exist matrices $\boldsymbol{\Pi}$ and $\boldsymbol{\Gamma}$ which solve the regulator equations, as:

$$\boldsymbol{\Pi S} = \boldsymbol{A\Pi} + \boldsymbol{B\Gamma} + \boldsymbol{P} \tag{16}$$

$$\boldsymbol{0} = \boldsymbol{C\Pi} + \boldsymbol{Q} \tag{17}$$

As a result, the full-information feedback controller for achieving goals *R1)* and *R2)* is given by:

$$\boldsymbol{u} = \boldsymbol{Kx} + (\boldsymbol{\Gamma} - \boldsymbol{K\Pi})\boldsymbol{d} \tag{18}$$

where $\boldsymbol{K}$ is selected so that all the eigenvalues of $\boldsymbol{A} + \boldsymbol{BK}$ are located on the open left-half plane. The gain matrix $\boldsymbol{L}$ in (15) is computed by $\boldsymbol{\Pi} \in \boldsymbol{R}^{r\times s}$ and $\boldsymbol{\Gamma} \in \boldsymbol{R}^{p\times s}$.

However, it is not practically feasible because not all of the state $\boldsymbol{x}$ can be measured. Thus, the feedback controller (18) needs to be refined using only the measurable signal e. Under the assumption *A3)*, an observer is constructed, driven by the measured error e, to achieve asymptotically tracking $(\boldsymbol{x}, \boldsymbol{d})$. The error feedback controller can be designed in the form of:

$$\begin{aligned} \dot{\boldsymbol{\xi}} &= \boldsymbol{F\xi} + \boldsymbol{Ge} \\ \boldsymbol{u} &= \boldsymbol{H\xi} \end{aligned} \tag{19}$$

with $\boldsymbol{\xi} = \mathrm{col}(\widehat{\boldsymbol{x}}, \widehat{\boldsymbol{d}})$ for tracking $\boldsymbol{x}$ and $\boldsymbol{d}$ asymptotically and the gain matrices $(\boldsymbol{F},\boldsymbol{G},\boldsymbol{H})$. Equation (19) can be written in transfer function form as:

$$\boldsymbol{T}(s) = \boldsymbol{H}(s\boldsymbol{I} - \boldsymbol{F})^{-1}\boldsymbol{G} \tag{20}$$

By the detectability of *A3)*, the observer is designed in the following form to estimate $(\boldsymbol{x}, \boldsymbol{d})$ using only the error signal $\boldsymbol{e}$, as:

$$\begin{bmatrix} \dot{\hat{\boldsymbol{x}}} \\ \dot{\hat{\boldsymbol{d}}} \end{bmatrix} = \left(\begin{bmatrix} \boldsymbol{A} & \boldsymbol{P} \\ \boldsymbol{0} & \boldsymbol{S} \end{bmatrix} - \begin{bmatrix} \boldsymbol{G_1} \\ \boldsymbol{G_2} \end{bmatrix} \begin{bmatrix} \boldsymbol{C} & \boldsymbol{Q} \end{bmatrix} \right) \begin{bmatrix} \hat{\boldsymbol{x}} \\ \hat{\boldsymbol{d}} \end{bmatrix} + \begin{bmatrix} \boldsymbol{G_1} \\ \boldsymbol{G_2} \end{bmatrix} \boldsymbol{e} + \begin{bmatrix} \boldsymbol{B} \\ \boldsymbol{0} \end{bmatrix} \boldsymbol{u} \tag{21}$$

with the pair $(\boldsymbol{G_1}, \boldsymbol{G_2})$ designed such that all the eigenvalues of $\left(\begin{bmatrix} \boldsymbol{A} & \boldsymbol{P} \\ \boldsymbol{0} & \boldsymbol{S} \end{bmatrix} - \begin{bmatrix} \boldsymbol{G_1} \\ \boldsymbol{G_2} \end{bmatrix} \begin{bmatrix} \boldsymbol{C} & \boldsymbol{Q} \end{bmatrix} \right)$ are in $\mathbb{C}^-$.

Replacing $(\boldsymbol{x}, \boldsymbol{d})$ with $\left(\widehat{x}, \widehat{d}\right)$ in the feedback controller (15), the error feedback controller is obtained by:

$$\begin{aligned} \begin{bmatrix} \dot{\hat{\boldsymbol{x}}} \\ \dot{\hat{\boldsymbol{d}}} \end{bmatrix} &= \begin{bmatrix} \boldsymbol{A} - \boldsymbol{G_1C} + \boldsymbol{BK} & \boldsymbol{P} - \boldsymbol{G_1Q} + \boldsymbol{B}(\boldsymbol{\Gamma} - \boldsymbol{K\Pi}) \\ -\boldsymbol{G_2C} & \boldsymbol{S} - \boldsymbol{G_2Q} \end{bmatrix} \\ &\quad \begin{bmatrix} \hat{\boldsymbol{x}} \\ \hat{\boldsymbol{d}} \end{bmatrix} + \begin{bmatrix} \boldsymbol{G_1} \\ \boldsymbol{G_2} \end{bmatrix} \boldsymbol{e} \\ \boldsymbol{u} &= \begin{bmatrix} \boldsymbol{K} & (\boldsymbol{\Gamma} - \boldsymbol{K\Pi}) \end{bmatrix} \begin{bmatrix} \hat{\boldsymbol{x}} \\ \hat{\boldsymbol{d}} \end{bmatrix} \end{aligned} \tag{22}$$

As a result, the gain matrices $(\boldsymbol{F},\boldsymbol{G},\boldsymbol{H})$ are obtained based on (19) and (22), as:

$$\boldsymbol{F} = \begin{bmatrix} \boldsymbol{A} - \boldsymbol{G_1C} + \boldsymbol{BK} & \boldsymbol{P} - \boldsymbol{G_1Q} + \boldsymbol{B}(\boldsymbol{\Gamma} - \boldsymbol{K\Pi}) \\ -\boldsymbol{G_2C} & \boldsymbol{S} - \boldsymbol{G_2Q} \end{bmatrix} \in \boldsymbol{R}^{(r+s)\times(r+s)}$$

$$\boldsymbol{G} = \begin{bmatrix} \boldsymbol{G_1} \\ \boldsymbol{G_2} \end{bmatrix} \in \boldsymbol{R}^{(r+s)\times q}, \boldsymbol{H} = \begin{bmatrix} \boldsymbol{K} & (\boldsymbol{\Gamma} - \boldsymbol{K\Pi}) \end{bmatrix} \in \boldsymbol{R}^{p\times(r+s)}$$

Compared with the full-information feedback controller (18) in which the state $\boldsymbol{x}$ and disturbance signal $\boldsymbol{d}$ are indispensable, the error feedback controller (22) is able to achieve the control objectives *R1)* and *R2)* using only the measurable error signal $\boldsymbol{e}$. In addition, the output $\boldsymbol{y} = \boldsymbol{Cx}$ can be regulated to track the reference signal $\boldsymbol{y_r} = -\boldsymbol{Qd}$ via measurement feedback.

4.3 Implementation of the demand side controller

The design procedure of the regulator-theory-based demand side controller is presented as follows.

1. *Model the exosystem matrix* $\boldsymbol{S}$. As discussed in Sect. 4.1, the exosystem system can be described as (14). In this work, short-term wind power forecast-

ing data is used as a period of wind power fluctuation signal $\boldsymbol{d}$. Normally, the forecasting models can be divided into statistical models and physical models. Statistical models provide an extrapolation of the future time-series by building the mathematical functions based on historical data analysis, such as the autoregressive (AR) model [27]. For physical models, the numerical weather prediction (NWP) model is applied widely to predict future wind power in which its root mean square error (RMSE), between the actual value and the forecasted value, can be decreased below 15% [28]. In view of the requirement of practical application, the NWP model is adopted in this paper to predict the curve of a period of wind power.

2. *Check the assumptions A1)–A3) for the controlled plant* (9). Note that the eigenvalues of the matrix $\boldsymbol{S}$ [see in (19)] are located on the imaginary axis. Hence, the assumption *A1)* holds in this paper. Check the stabilizing ability of $(\boldsymbol{A}, \boldsymbol{B})$ and the detectability of $\left(\begin{bmatrix} \boldsymbol{A} & \boldsymbol{P} \\ 0 & S \end{bmatrix}, \begin{bmatrix} C & Q \end{bmatrix}\right)$ by using the PBH test below to compute the rank condition, as:

$$\begin{aligned} &Rank\left(\begin{bmatrix} \lambda \boldsymbol{I} - \boldsymbol{A} & \boldsymbol{B} \end{bmatrix}\right) = n_A = 3m \\ &Rank\left(\begin{bmatrix} \mu \boldsymbol{I} - \begin{bmatrix} \boldsymbol{A} & \boldsymbol{P} \\ \boldsymbol{0} & \boldsymbol{S} \end{bmatrix} \\ \begin{bmatrix} \boldsymbol{C} & \boldsymbol{Q} \end{bmatrix} \end{bmatrix}\right) = n_{APS} = 1 + 2N + 3m \end{aligned} \tag{23}$$

where n_A and n_{APS} are the dimensions of the corresponding system, and λ and μ are the eigenvalues of the matrices $\boldsymbol{A}$ and $\begin{bmatrix} \boldsymbol{A} & \boldsymbol{P} \\ \boldsymbol{0} & \boldsymbol{S} \end{bmatrix}$ sitting on the closed right-half plane, respectively.

3. *Select gain matrix $\boldsymbol{K}$ based on linear quadric (LQ) optimal control.* If *A1)–A3)* hold, find a gain matrix $\boldsymbol{K}$ such that all the eigenvalues of the matrix $\boldsymbol{A} + \boldsymbol{BK}$ are assigned on the left-half plane. In this paper, the LQ method is used to select an optimal gain matrix $\boldsymbol{K}$ so that the control objectives are achieved and the dynamic performance of the controller is guaranteed. For the controlled plant (9), the LQ cost function is:

$$\boldsymbol{J} = \int_0^{\infty} \left(\boldsymbol{y}^T \boldsymbol{Q}_{lq} \boldsymbol{y} + \boldsymbol{u}^T \boldsymbol{R}_{lq} \boldsymbol{u}\right) dt \tag{24}$$

where the weighting matrices $\boldsymbol{Q}_{lq} \in \boldsymbol{R}^{q \times q}$ and $\boldsymbol{R}_{lq} \in \boldsymbol{R}^{p \times p}$ are selected so that a trade-off is considered between minimizing the tie-lie power fluctuation $\boldsymbol{y}$ and optimizing the dynamic performance of the EALs (vector $\boldsymbol{u}$). Based on the standard LQ control method, the feedback gain matrix $\boldsymbol{K}$ is obtained by solving the following algebraic equation:

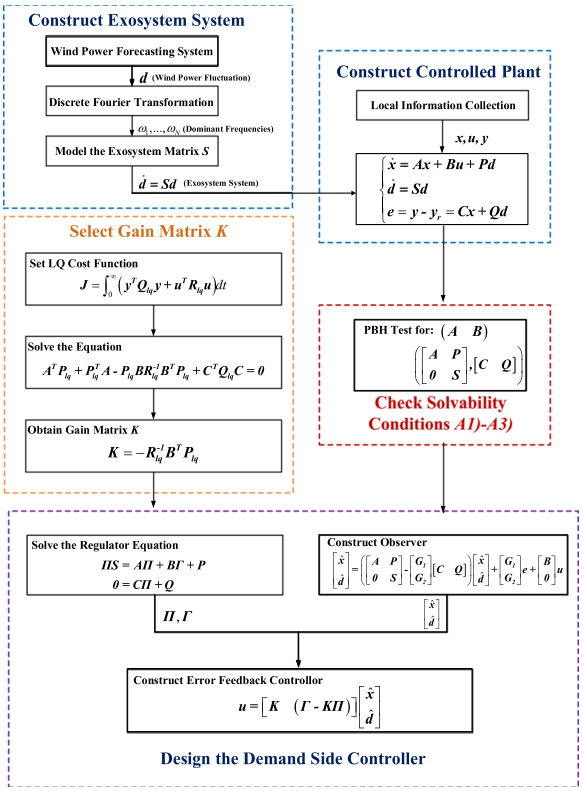

Fig. 6 The diagram of the regulator-theory-based control scheme

$$\boldsymbol{A}^T \boldsymbol{P}_{lq} + \boldsymbol{P}_{lq}^T \boldsymbol{A} - \boldsymbol{P}_{lq} \boldsymbol{B} \boldsymbol{R}_{lq}^{-1} \boldsymbol{B}^T \boldsymbol{P}_{lq} + \boldsymbol{C}^T \boldsymbol{Q}_{lq} \boldsymbol{C} = \boldsymbol{0} \tag{25}$$

$$\boldsymbol{K} = -\boldsymbol{R}_{lq}^{-1} \boldsymbol{B}^T \boldsymbol{P}_{lq} \tag{26}$$

Note that the weighting matrices $\boldsymbol{Q}_{lq}$ and $\boldsymbol{R}_{lq}$ can be selected flexibly according to the required control performance on the demand side.

4. *Construct the demand side controller.* Solve the regulator Eqs. (16)–(17) and find the solutions of the matrices $\boldsymbol{\Pi}$ and $\boldsymbol{\Gamma}$. Construct the observer (21) and design the error feedback controller (22) by steps discussed in Sect. 4.2.

The detailed design procedure of the regulator-theory-based demand side control scheme is illustrated in Fig. 6. The feedback controller is constructed using local state variables and a remote disturbance signal. The results of the time domain simulation will be presented in the next section to validate its effectiveness.

5 Simulations and analysis

To verify the performance of the proposed demand side controller (22), an actual electrolytic aluminum IMG in Inner Mongolia, China is considered as the case study

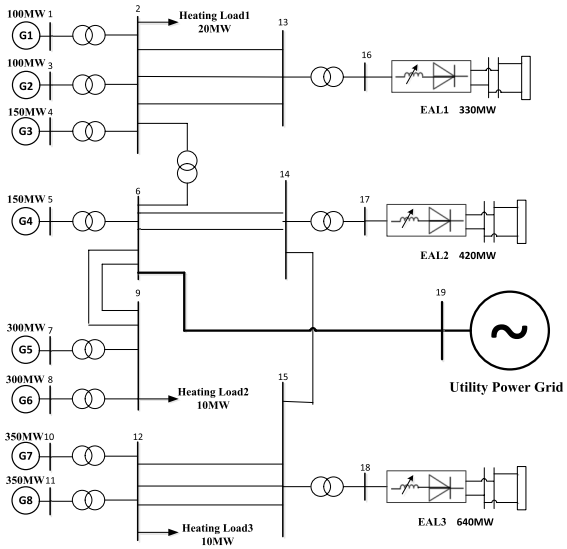

Fig. 7 The structure of an actual IMG with the EALs

[13–15]. The structure of the IMG is shown in Fig. 7. The demand side includes three production lines (EAL1–EAL3, 1390 MW in all) and 40 MW heating loads. The electrical energy that the aluminum loads need is from two sources: (1) eight coal-fired thermal generators (G1–G8) with a total capacity of 1800 MW; and (2) transmission power P_{tie} from the tie-line that is connected with the UPG.

Simulations are conducted on a real-time digital simulator (RTDS) platform and MATLAB. RTDS is a type of real-time hardware platform to study electromagnetic transient phenomena in power systems. The models of the power systems are constructed on RTDS, including the detailed model of the electrolytic aluminum loads. Once the demand side control strategy is activated, based on the real-time computation, the state variables $\boldsymbol{x}$, disturbance $\boldsymbol{d}$ and error $\boldsymbol{e}$ of the power systems are fed to MATLAB within every setting time step via specific signal transmission channels. The proposed demand side controllers (22) are designed within each time step in MATLAB according to the instructions in Sect. 4.3. After calculating the demand side controllers, the control input $\boldsymbol{u}$ is transmitted to the RTDS platform. Then, the demand side (the electrolytic aluminum loads) carries out the proposed control strategy based on the control input $\boldsymbol{u}$. This means the DC current references $\Delta \boldsymbol{I}_{\boldsymbol{DCref}j}$ of the electrolytic aluminum loads will be regulated. In the next time steps, the above instructions are repeated until the end of the simulation.

The basic information of the IMG has been introduced in Sect. 2. The two-area power system and IEEE 68-bus power system are selected as the UPG and connected with the IMG, respectively.

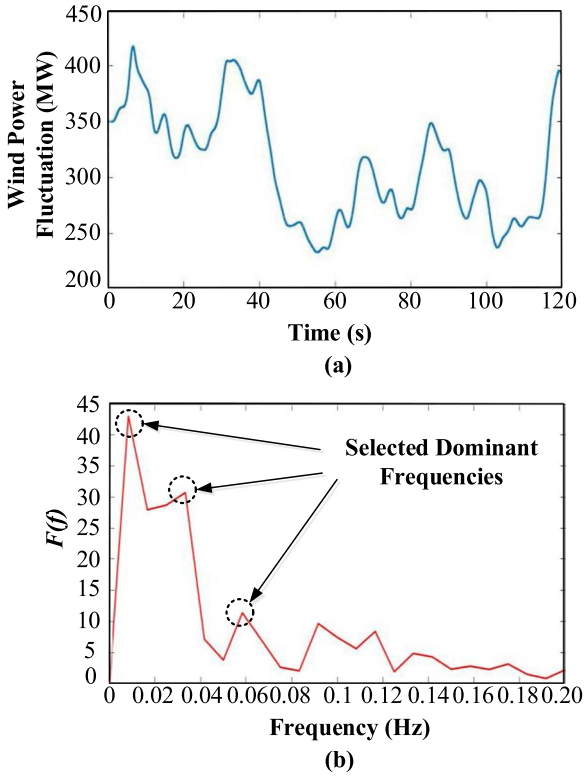

Fig. 8 **a** The wind power fluctuation in a typical operating scenario, **b** The frequency spectrum of the wind power fluctuation

As discussed in Sect. 3.1, the DC current of the EALs is normally constant, and thus the active power consumption P_{EAL} of the EALs remains stable. In this paper, the DC current I_{DC} of the EALs is regulated by controlling the voltage drop U_{SR} on the saturable reactors, and consequently. P_{EAL} is controllable. In the case of the two-area power system, the performance of the proposed demand side controller is verified by comparing with the constant current control scheme (i.e., no active power control on P_{EAL}). By comparing with the other control method, the simulation results in the case of the IEEE 68-bus power system illustrate the effectiveness of the proposed demand side controller in minimizing steady-state error. In addition, the results indicate that the proposed wide area closed-loop demand side control method is also applicable to large power systems.

5.1 Formulating the demand side controller

In this section, a typical operating scenario of a wind farm is selected as the case study. The short-term wind power fluctuation is predicted by the forecasting system, shown in Fig. 8a. With the help of discrete Fourier

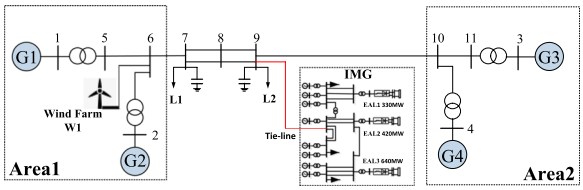

Fig. 9 Two-area power system connected with the IMG

transformation (DFT), the frequency spectrum of the wind power fluctuation is analyzed and presented in Fig. 8b. Three dominant frequencies (0.0083 Hz, 0.0333 Hz and 0.0583 Hz) are chosen to characterize the wind power fluctuation. Hence, the exosystem matrix S is computed in the form of (14) by the three dominant frequencies.

By virtue of WAMS, the measurable error signal $\boldsymbol{e}$ (i.e., $\boldsymbol{e} = \Delta P_{tie} - \Delta P_w$) is selected as the feedback signal for the proposed demand side controller. The weighting matrices in (24) are selected, by trial and error, as $\boldsymbol{Q_{lq}} = 15$ and $\boldsymbol{R_{lq}} = diag(10, 7, 5)$. Using the LQ optimal control method, the gain matrix $\boldsymbol{K}$ is obtained as:

$$\boldsymbol{K} = \begin{bmatrix} -0.29 & -0.48 & -0.53 & 3.89 & 3.11 & 3.40 & 4.62 & 4.32 & 4.05 \\ -0.25 & -0.46 & -0.52 & 3.53 & 3.09 & 3.38 & 4.56 & 4.25 & 4.02 \\ -0.24 & -0.43 & -0.50 & 3.44 & 3.03 & 3.31 & 4.51 & 4.19 & 3.98 \end{bmatrix}$$

Based on the output regulator theory in Sect. 4, after solving $(\boldsymbol{\Pi}, \boldsymbol{\Gamma})$ for the regulator Eqs. (16)–(17) and computing gain matrices (F, G, H), the error feedback controller can be obtained in the form of (20) or (22).

5.2 Two-area power system

As shown in Fig. 9, in the two-area power system, the IMG is connected on Bus 9 via a tie-line. There are three generation units in Area 1 (i.e., G1, G2 and W1) and two in Area 2 (i.e., G3 and G4). The initial active power of the generators and loads is listed in Table 1. As introduced in Sect. 2, the EALs are supplied by the generators in the IMG and the UPG. As a result, the active power on the tie-line P_{tie} reaches 400 MW. In this case, to verify the effectiveness of the proposed control method, the two following scenarios are considered:

Table 1 The initial output active power of the generators and loads in the two-area power system

Generators	G1	690 MW
	G2	380 MW
	G3	700 MW
	G4	700 MW
	W1	350 MW
Loads	L1	960 MW
	L2	1360 MW

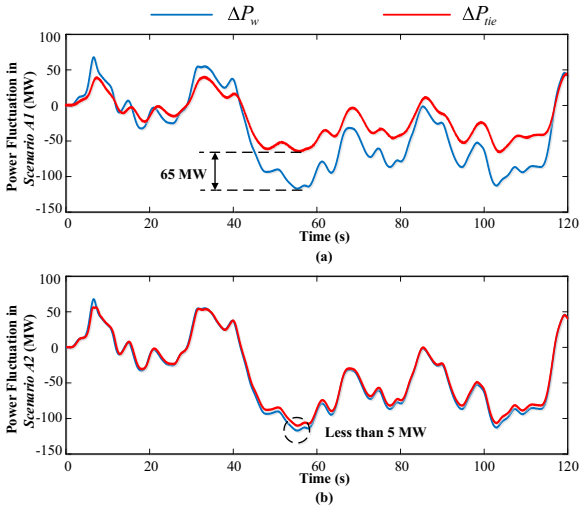

Fig. 10 The wind power fluctuation ΔP_w and active power deviation on tie-line ΔP_{tie}. **a** The power curves in *Scenario A1*, **b** the power curves in *Scenario A2*

1. *Scenario A1*: the constant current control method on demand side (P_{EALj} is not regulated), which serves as the base case for comparison.
2. *Scenario A2*: the proposed regulator-theory-based demand side control method.

In the normal condition (*Scenario A1*), the EALs works at constant current control mode to ensure the production.

The aim of the proposed regulator-theory-based demand side control scheme is to achieve the active power deviation on the tie-line ΔP_{tie} to track the wind power fluctuation ΔP_w. The simulation results in *Scenario A1* and *Scenario A2* are presented in Figs. 10 and 11. In *Scenario A1*, the active power consumption of the EALs is maintained at a steady level ($\Delta P_{EAL} \approx 0$, as shown in Fig. 11a). Taking EAL1 as an example, the initial voltage drop on the saturable reactor ΔU_{SR1} is about 38 V. Because of the fast response of the saturable reactor, ΔU_{SR1} changes within 20–50 V and the DC current I_{DC1} remains at 326 kA in *Scenario A1*. When the proposed demand side control method is applied, I_{DC1} changes within 310–335 kA (ΔU_{SR1} fluctuates within 20–70 V), leading ΔP_{EAL} to be regulated from 50 MW to − 100 MW in *Scenario A2*.

The simulation results of the two different demand side control methods illustrated in Fig. 10 show that, in *Scenario A1*, the active power deviation ΔP_{tie} is not able to track the wind power fluctuation ΔP_w because the power consumption of the EALs ΔP_{EAL} is not regulated. As a result, the maximum deviation between ΔP_{tie} and ΔP_w reaches 65 MW. However, in *Scenario A2*, the proposed

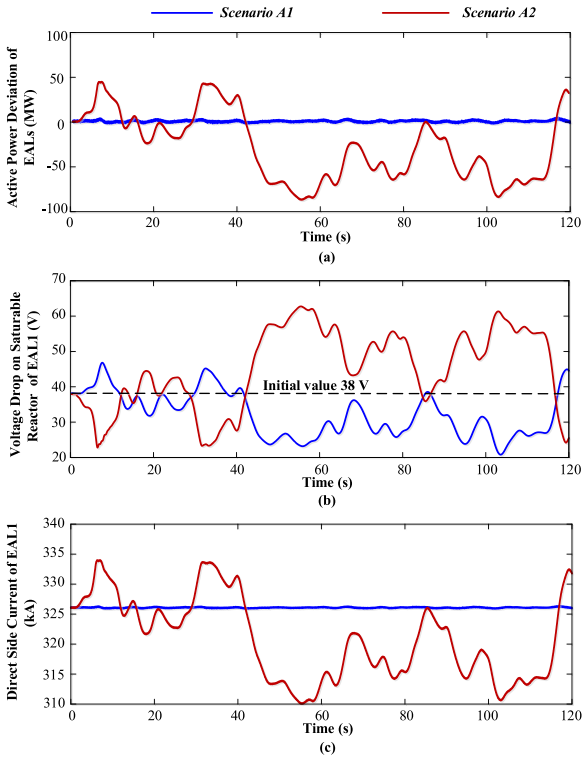

Fig. 11 **a** The active power deviation of EALs ΔP_{EAL} in *Scenario A1* and *Scenario A2*, **b** The voltage drop on saturable reactor of EAL1 ΔU_{SR1} in *Scenario A1* and *Scenario A2*

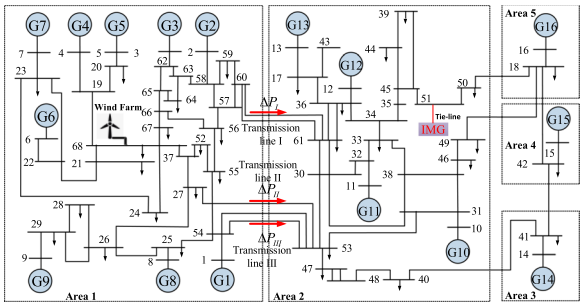

Fig. 12 IEEE 68-bus power system connected with the IMG

regulator-theory-based demand side control method ensures that ΔP_{EAL} is regulated according to the wave of ΔP_w. Consequently, ΔP_{tie} is able to track ΔP_w with the error being less than 5 MW. This provides an obvious proof of direct wind power purchase for the large industrial consumers.

In summary, by comparing with the constant DC current control method, the proposed demand side control scheme shows an evident effect on error regulation and keeping the control system stable *(R1)* and *(R2)* in Sect. 4. Based on output regulator theory, ΔU_{SR1} is controlled by giving the DC current reference signal ΔI_{DCref1} according to the control objective (i.e., tracking the error signal). Compared with the constant current control scheme, the change range of ΔU_{SR1} is much wider in the proposed control scheme.

5.3 IEEE 68-bus power system

The effectiveness of the proposed demand side control scheme has been verified in the simulation of the two-area power system. To further validate the control effects of the proposed demand side control scheme in large power systems, the IEEE 68-bus power system (known as the New England and New York interconnected system), as shown in Fig. 12, is selected as the case study. The wind farm W1 is connected to Bus-68, with an initial active power of 350 MW. The wind power fluctuation is shown in Fig. 8a. The IMG in Fig. 7 is connected to Bus 51 via a tie-line.

Three scenarios are studied to test the proposed demand side control method by comparing with other methods:

1. *Scenario B1*: the constant current control method on the demand side.
2. *Scenario B2*: the PI control method on the demand side.
3. *Scenario B3*: the proposed regulator-theory-based demand side control method.

In the IEEE 68-bus power system, there are three transmission lines between Area 1 and Area 2, denoted as transmission line I (Bus-60 to Bus-61), II (Bus-27 to Bus-53) and III (Bus-54 to Bus-53). The active power fluctuations on transmission line I, II and III are ΔP_I, ΔP_{II} and ΔP_{III}, respectively. The power flow between Area 1 and Area 2 is denoted as P_{A1-A2}. Clearly, the wind power fluctuation ΔP_w leads to the power change ΔP_{A1-A2} on the power flow between Area 1 and Area 2.

According to the simulation in Sect. 5.2, when the constant current control method on the demand side is applied, the active power consumption of the EALs is not regulated. The simulation results in *Scenario B1* are presented in Fig. 13.

In *Scenario B1*, ΔP_{A1-A2} is the sum of the active power fluctuations on transmission lines I, II and III, i.e., $\Delta P_{A1-A2} = \Delta P_I + \Delta P_{II} + \Delta P_{III}$, as presented in Fig. 13a. When P_{EAL} remains at a constant value, the power fluctuation on the tie-line ΔP_{tie} is not able to track ΔP_w, as shown in Fig. 13b. The deviation between ΔP_w and ΔP_{tie} is significant, which means the direct wind power purchasing strategy is not suitable for the extreme short-term wind power fluctuation scenarios if no extra control methods are applied.

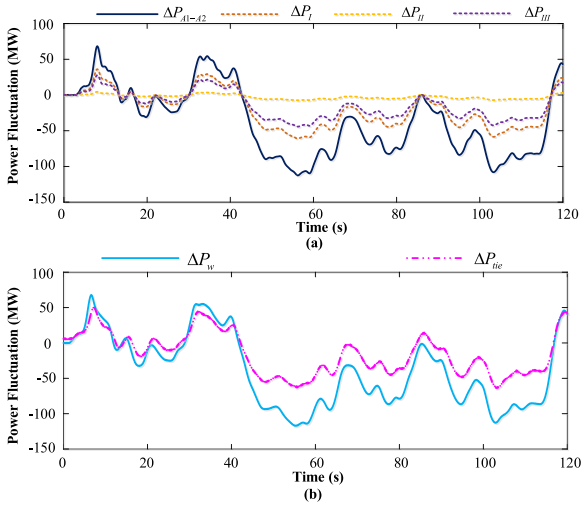

Fig. 13 Simulation results in *Scenario B1*. **a** The active power fluctuations on transmission lines between Area 1 and Area 2, **b** the wind power fluctuation and the power fluctuation on the tie-line

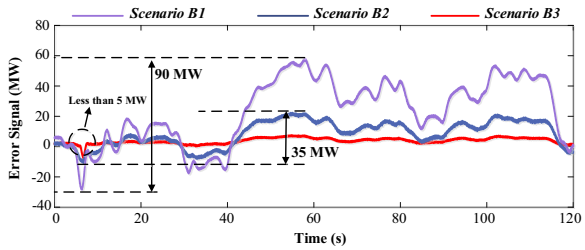

Fig. 14 The error signal *e* in three scenarios

Figure 14 depicts the error signal $\boldsymbol{e}$ (i.e., $\boldsymbol{e} = \Delta P_{tie} - \Delta P_w$) in the three scenarios. In *Scenario B3*, the proposed regulator-theory-based demand side controller is constructed using error signal and local information. As a comparison, the PI control scheme in *Scenario B2* introduces the wind power fluctuation ΔP_w and uses local PI controllers of the EALs. Based on the simulation results, the error can be controlled within 5 MW with the proposed demand side controller (*Scenario B3*). This represents a good dynamic response via coordinating the three EALs with an optimal gain matrix $\boldsymbol{K}$. By comparison, the PI controllers using the remote signal ΔP_w as a feedback signal show a poor dynamic performance in decreasing $\boldsymbol{e}$, leading the maximum deviation of the error to reach about 35 MW. Therefore, the regulator-theory-based demand side controller is more effective than the PI control scheme in tracking the wind power fluctuation in a large system. For this reason, the proposed demand side control scheme presents an applicable effort for the EALs to participate in the direct wind power purchasing market.

6 Conclusion

The basic structure of the direct wind power purchasing mode for grid-connected IMG has been studied. Because of the fast response and considerable regulation capacity of the EALs, the short-term wind power fluctuations can be tracked via regulating the active power consumption of the EALs. With the use of WAMS, a wide area closed-loop demand side control architecture is proposed to regulate the power consumption of the EALs. The demand side control is formulated as an output regulation problem. Based on output regulator theory, a demand side controller is developed with only local state variables and a remote disturbance signal. The simulation results demonstrate the effectiveness of the proposed demand side controller on tracking the short-term time-varying wind power fluctuations. Future work will focus on the DWPP mode and control methods for multiple wind power sources and industrial consumers.

Acknowledgements
This work was supported by Science and Technology Project of State Grid Corporation of China (5100-202199286A-0-0-00). Appreciation to my co-authors who involved with the work.

Author contributions
The paper was a collaborative effort among the authors. Y.Z. Sun conceived the idea and provided technical guidance required for completing the study. X. Ding formulated the algorithms, carried out the simulation studies, and finished the paper. S.Y. Liao carried out simulation studies and improved the paper quality. J. Xu provided technical suggestions and guidance and reviewed the manuscript. J.W. Zheng supplemented the simulation results and revised the paper. All authors read and approved the final manuscript.

Funding
This work was supported by Science and Technology Project of State Grid Corporation of China (5100-202199286A-0-0-00).

Availability of data and materials
The datasets used and analyzed during the current study are available from the corresponding author on reasonable request.

Declarations

Competing interests
The authors declare that they have no known competing financial interests or personal relationships that could have appeared to influence the work reported in this paper.

Author details
[1]School of Electrical Engineering and Automation, Wuhan University, Wuhan 430072, China. [2]School of Mechanical Engineering, University of Shanghai for Science and Technology, Shanghai, China. [3]State Grid Hubei Electric Power Research Institute, State Grid Hubei Electric Power Co., Ltd., Wuhan, China.

Received: 22 June 2022 Accepted: 15 November 2022
Published online: 13 December 2022

References

1. National Energy Administration released the statistical data of the national power industry in 2021. http://www.nea.gov.cn/2022-01/26/c_1310441589.htm. Accessed 26 Jan 2022.
2. Li, G., Li, G., & Zhou, M. (2019). Model and application of renewable energy accommodation capacity calculation considering utilization level of inter-provincial tie-line. *Protection and Control of Modern Power Systems, 4*(1), 1–12.
3. Li, Z., Wu, W., Shahidehpour, M., & Zhang, B. (2016). Adaptive robust tie-line scheduling considering wind power uncertainty for interconnected power systems. *IEEE Transactions on Power Systems, 31*(4), 2701–2713.
4. Huang, H., Du, Y., Song, S., & Guo, Y. (2020). Key technologies and economic analysis of decentralized wind power consumption: A case study in b city, China. *Energies, 13*(16), 4147.
5. Liao, S., Xu, J., Sun, Y., & Bao, Y. (2018). Local utilization of wind electricity in isolated power systems by employing coordinated control scheme of industrial energy-intensive load. *Applied Energy, 217*, 14–24.
6. Zhao, X., Lyon, T. P., & Song, C. (2012). Lurching towards markets for power: China's electricity policy 1985–2007. *Applied Energy, 94*, 148–155.
7. Zeng, M., Yang, Y., Fan, Q., Liu, Y., & Zou, Z. (2015). Coordination between clean energy generation and thermal power generation under the policy of "direct power-purchase for large users" in China. *Utilities Policy, 33*, 10–22.
8. Zhang, W., Wang, X., Wu, X., & Yao, L. (2015). An analysis model of power system with large-scale wind power and transaction mode of direct power purchase by large consumers involved in system scheduling. *Proceedings of the Chinese Society of Electrical Engineering, 35*(12), 2927–2935.
9. Zhao, J., Wang, J., & Su, Z. (2014). Power generation and renewable potential in China. *Renewable & Sustainable Energy Reviews, 40*, 727–740.
10. Feng, L., Zhang, J., Li, G., & Zhang, B. (2016). Cost reduction of a hybrid energy storage system considering correlation between wind and PV power. *Protection and Control of Modern Power Systems, 1*(11), 1–9.
11. Liao, S., Jian, X., Sun, Y., Yi, B., & Tang, B. (2018). Control of energy-intensive load for power smoothing in wind power plants. *IEEE Transactions on Power Systems, 33*(6), 6142–6154.
12. Zhang, C., Lin, W., Ke, D., & Sun, Y. (2019). Smoothing tie-line power fluctuations for industrial microgrids by demand side control: An output regulation approach. *IEEE Transactions on Power Systems, 34*(5), 3716–3728.
13. Cui, T., Lin, W., Sun, Y., Xu, J., & Zhang, H. (2016). Excitation voltage control for emergency frequency regulation of island power systems with voltage-dependent loads. *IEEE Transactions on Power Systems, 31*(2), 1204–1217.
14. Xu, J., Liao, S., Sun, Y., Ma, X., Gao, W., & Li, X. (2014). An isolated industrial power system driven by wind-coal power for aluminum productions: A case study of frequency control. *IEEE Transactions on Power Systems, 30*(1), 471–483.
15. Bao, Y., Xu, J., Liao, S., Sun, Y., Li, X., & Jiang, Y. (2018). Field verification of frequency control by energy-intensive loads for isolated power systems with high penetration of wind power. *IEEE Transactions on Power Systems, 33*(6), 6098–6108.
16. Bao, Y., Xu, J., Feng, W., Sun, Y., Liao, S., & Yin, R. (2019). Provision of secondary frequency regulation by coordinated dispatch of industrial loads and thermal power plants. *Applied Energy, 241*, 302–312.
17. Said, S. M., Ali, A., & Hartmann, B. (2020). Tie-line power flow control method for grid-connected microgrids with SMES based on optimization and fuzzy logic. *Journal of Modern Power Systems and Clean Energy, 8*(5), 941–950.
18. Li, Z., Wu, W., Shahidehpour, M., & Zhang, B. (2015). Adaptive robust tie-line scheduling considering wind power uncertainty for interconnected power systems. *IEEE Transactions on Power Systems, 31*(4), 2701–2713.
19. Dan, W., Ge, S., Jia, H., Wang, C., & Kong, X. (2014). A demand response and battery storage coordination algorithm for providing microgrid tie-line smoothing services. *IEEE Transactions on Sustainable Energy, 5*(2), 476–486.
20. Xu, Y., Li, F., Jin, Z., & Variani, M. H. (2016). Dynamic gain-tuning control (DGTC) approach for AGC with effects of wind power. *IEEE Transactions on Power Systems, 31*(5), 3339–3348.
21. Pouya, B., Qobad, S., & Hassan, & Bevrani. (2016). Intelligent demand response contribution in frequency control of multi-area power systems. *IEEE Transactions on Smart Grid, 9*(2), 1282–1291.
22. Isidori, A., & Byrnes, C. I. (1990). Output regulation of nonlinear systems. *IEEE Transactions on Automatic Control, 35*(2), 131–140.
23. Wei, L., & Dai, L. (1996). Solutions to the output regulation problem of linear singular systems. *Automatica, 32*(12), 1713–1718.
24. Appasani, B., Jha, A. V., Mishra, S. K., & Ghazali, A. N. (2021). Communication infrastructure for situational awareness enhancement in WAMS with optimal PMU placement. *Protection and Control of Modern Power Systems, 6*(9), 1–12.
25. Sun, Y., Liao, S., Xu, J., & Gu, R. (2016). Industrial implementation of a wide area measurement system based control scheme in an isolated power system driven by wind–coal power for aluminum productions. *IET Generation Transmission & Distribution, 10*(8), 1877–1882.
26. Lin, J., Sun, Y., Sorensen, P., Li, G., & Gao, W. (2012). Method for assessing grid frequency deviation due to wind power fluctuation based on "time-frequency transformation." *IEEE Transactions on Sustainable Energy, 3*(1), 65–73.
27. Lydia, M., Kumar, S. S., Selvakumar, A. I., & Kumar, G. E. P. (2016). Linear and non-linear autoregressive models for short-term wind speed forecasting. *Energy Conversion and Management, 112*, 115–124.
28. Xu, Q., He, D., Zhang, N., Kang, C., Xia, Q., & Bai, J. (2015). A short-term wind power forecasting approach with adjustment of numerical weather prediction input by data mining. *IEEE Transactions on Sustainable Energy, 6*(4), 1283–1291.

Submit your manuscript to a SpringerOpen journal and benefit from:

- ► Convenient online submission
- ► Rigorous peer review
- ► Open access: articles freely available online
- ► High visibility within the field
- ► Retaining the copyright to your article

Submit your next manuscript at ► springeropen.com